Journal of Alloys and Compounds 656 (2016) 530–538

Contents lists available at ScienceDirect

Journal of Alloys and Compounds

journal homepage: http://www.elsevier.com/locate/jalcom

Porous TiAl alloys fabricated by sintering of TiH_2 and Al powder mixtures

Qin Peng [a], Bin Yang [b], Libin Liu [c], Changjiang Song [c], Bernd Friedrich [a, *]

[a] IME Process Metallurgy and Metal Recycling, RWTH Aachen University, Intzestr. 3, 52056 Aachen, Germany
[b] Institute of Physics, University of Rostock, Wismarsche Straße 43-45, 18051 Rostock, Germany
[c] State Key Laboratory of Advanced Special Steels, Shanghai University, 149 Yanchang Road, 200072 Shanghai, PR China

ARTICLE INFO

Article history:
Received 12 August 2015
Received in revised form
28 September 2015
Accepted 30 September 2015
Available online 9 October 2015

Keywords:
Sintering
TiAl alloys
Porous metals

ABSTRACT

Porous TiAl alloys with different nominal powder compositions were fabricated through a cost-effective powder metallurgy (PM) approach by sintering TiH_2 and Al mixed powders. It is found that the pore properties vary with the TiH_2 and Al contents, i.e., the nature of the pores can be improved by using different compositions. Furthermore, by detailed structural characterizations, four crystalline phases, i.e., α_2-Ti_3Al, γ-TiAl, $TiAl_3$, and Ti_2Al_5, were observed in the fabricated porous TiAl alloys with different compositions. An optimal composition of TiH_2-50wt% Al is preferred since its maximum open porosity is about 70% and its viscous permeability coefficient for nitrogen is 1.11 μm^2.

1. Introduction

There is great interest in porous metals as potential engineering materials in various industrial fields, especially in filtration fields, due to their unique properties such as impact energy absorption capacity, thermal conductivity, electrical insulation, and, in particular, good gas and liquid permeability [1–4]. However, their potential applications in filtration fields, e.g., high-temperature liquid and gas separation, were limited due to their poor corrosion resistance, poor oxidation resistance, and poor burn resistance at high temperatures. After extensive investigation for more than three decades [5–8] and the pioneering work of H. Clemens et al. [9–11], the TiAl alloys can now be seen as innovative high-temperature engineering materials. The advantages of this class of alloys are their sound engineering performances, including good oxidation resistance at elevated temperatures, particularly temperatures higher than 750 °C, and their excellent acid/alkali corrosion resistance. Advanced TiAl alloys, especially γ-TiAl based alloys, are complex multi-phase alloys that can be manufactured and processed by ingot or powder metallurgy as well as precision casting methods [7,9]. However, applications in filtration fields have been severely limited due to the alloys' high intrinsic costs. In general, the sintering process of titanium-based objects should be performed in an argon or hydrogen atmosphere or in a vacuum due to titanium's high reactivity with oxygen, nitrogen, and water [12]. Therefore, cost reduction is a major driving force in the manufacturing and processing of porous TiAl alloys filters. On the other hand, the formation of titanium oxide or titanium nitride layers during sintering cannot be prevented completely under these neutral or reducing atmospheres. In order to prevent the formation of these compounds during the processing stage, the titanium hydride evolving hydrogen is an attractive raw material [12,13]. During sintering, the titanium hydride acts as a scavenger and reacts with oxide and nitrogen contaminants, resulting in titanium products that are protected against undesirable nitriding and oxidation [12].

Moreover, in the TiAl alloys system, different crystal structures, i.e., intermetallic compounds containing a mixture of metallic and covalent bonds [4], provide sound physical and chemical properties [8,9,14–17]. For example, the α_2-Ti_3Al phase (Al content, 14 to 23 wt %) has excellent corrosion resistivity; the γ-TiAl phase (Al content, 35 to 42 wt%) has low density and high-temperature structure stability; and the $TiAl_3$ phase (Al content, about 63 wt%) has good oxidation resistance and low density [18]. Consequently, it is worth investigating the effects of the Al content on pore structure and filter performance.

In this study, we introduce a new cost-effective powder metallurgy (PM) approach to fabricate porous TiAl alloys parts by

* Corresponding author.
E-mail address: bfriedrich@ime-aachen.de (B. Friedrich).

http://dx.doi.org/10.1016/j.jallcom.2015.09.259
0925-8388/

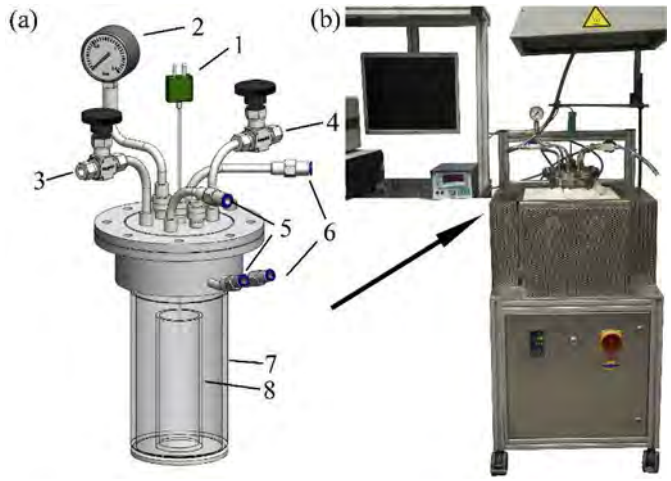

Fig. 1. (a) The schematic of the gas tight container for the sintering process: 1-Thermocouple, 2-Barometer, 3-Argon in, 4-Argon out, 5-Water in, 6-Water out, 7-Chamber, 8-Crucible. (b) The photograph of the sintering system.

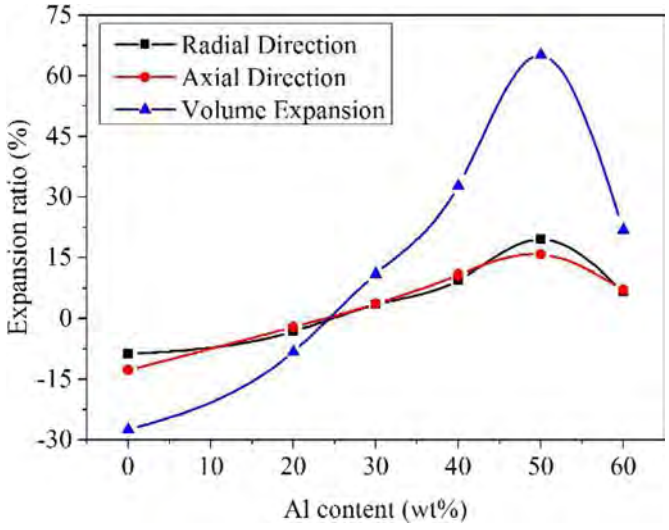

Fig. 3. The volume expansion of the compacts with the nominal composition of TiH_2-0wt% Al up to TiH_2-60wt% Al after sintering.

sintering TiH_2 and Al powders with a nominal composition range from TiH_2-20wt% Al to TiH_2-60wt% Al. The different phases with different Al contents were characterized and the resulting filtration properties, i.e., pore structure and gas permeability/filter performance, were discussed.

2. Material and methods

Commercially available Al powders (99.8% purity, $d_{50} = 55$ μm) and TiH_2 powders (Ti > 99.6 wt%, C = 0.015 wt%, Fe = 0.028 wt%, H = 3.80 wt%, O = 0.21 wt%, <63 μm, GfE, Germany) were used in the experiments. The d_{50} of TiH_2 powders is 33.91 μm. The nominal compositions varied from TiH_2-20wt% Al to TiH_2-60wt% Al with an increment of 10 wt% Al (TiH_2 content = 100% − Al content) in order to gain a systematic understanding of the relationship between the fabricated pore structures and different compositions. The reactant powders were first dry-mixed in a tumbler mixer for 18 h with the rolling rate of 60 rpm, followed by cold isostatic pressing (CIP, EPSI, Belgium) into compact cylinders using rubber tubes (Polyurethane, 50 duro, Trexler, USA) with a diameter of about 40 mm and a length of about 40 mm. The CIP pressure was 100 MPa and the duration time was 120 s.

The compact cylinder in an Al_2O_3 crucible was then put into a gas tight container, which was made of THERMAX heat-resistant steel (shown in Fig. 1(a)). Later, the container was put into the cavity of a cylindrical resistance furnace (shown in Fig. 1(b)). The temperature was measured using a thermocouple in the container, and the sintering process was protected by flowed argon with the rate of 20 ml/min. In Fig. 2, the temperature profile (sintering temperature vs. sintering time) is illustrated, and the two holding platforms are indicated. In order to avoid cracks in the compact cylinder caused by continuous heating at high heating rates, the cylinder was sintered with stepped heating at a heating rate of 5 °C/min. For the first holding platform, the cylinder was kept at 630 °C for 120 min, because it is close but lower than the melting point of Al (660 °C), at which cracks can be eliminated and the original shape of the cylinder can be preserved. Moreover, TiH_2 can be decomposed completely into highly reactive Ti and H_2 [19]. For the second holding platform, the cylinder was kept at 1200 °C for 60 min. The cylinder was then cooled down in the furnace.

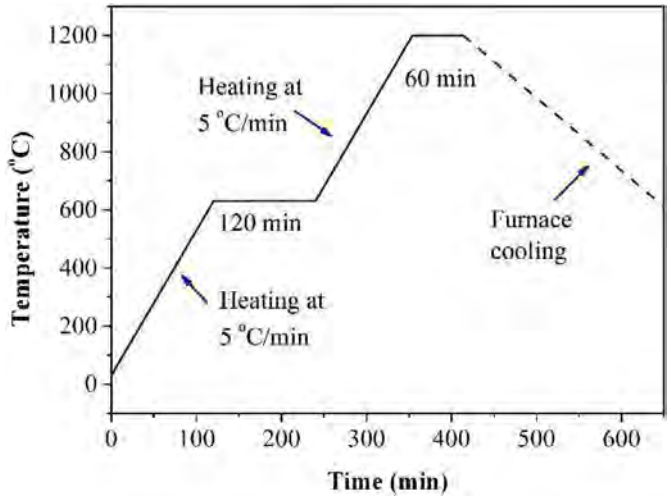

Fig. 2. The sintering temperature as a function of sintering time.

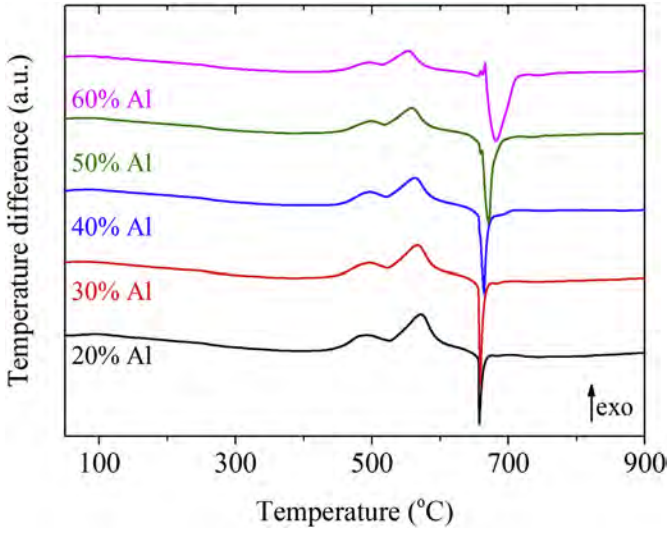

Fig. 4. DTA plots of the TiH_2–Al powder mixtures with different Al contents.

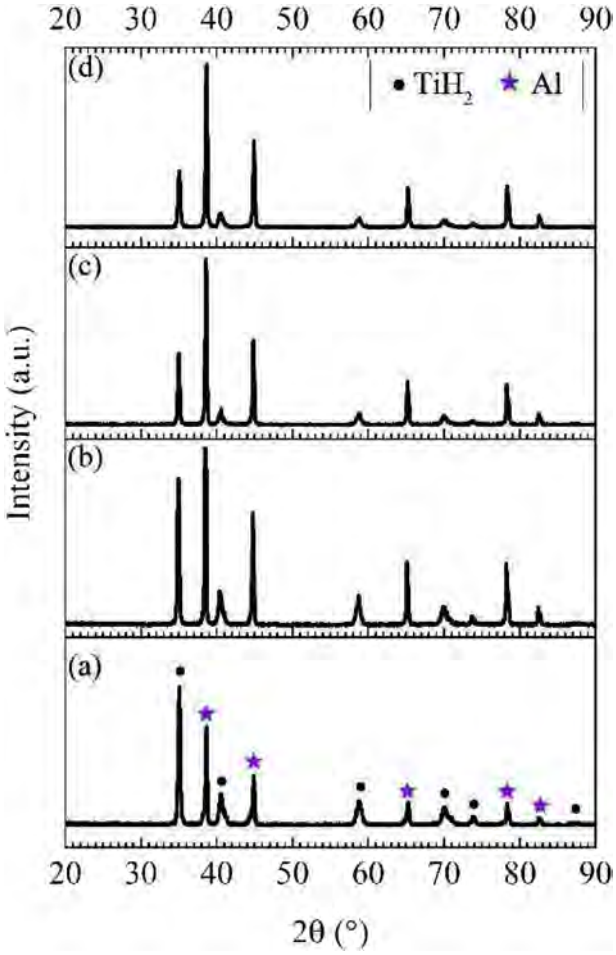

Fig. 5. X-ray patterns of green cylinders after CIP: (a) TiH_2-20wt% Al, (b) TiH_2-40wt% Al, (c) TiH_2-50wt% Al, (d) TiH_2-60wt% Al.

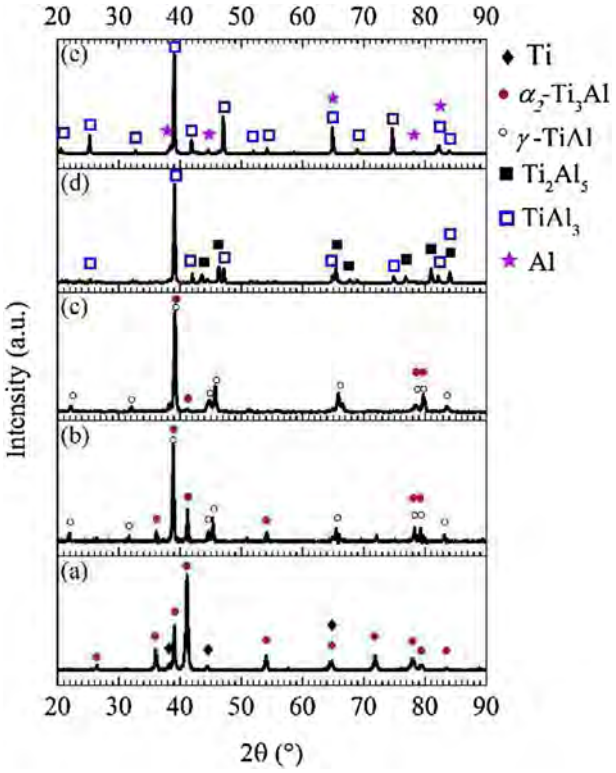

Fig. 6. X-ray patterns of porous TiAl alloy cylinders with different compositions: (a) TiH_2-20wt% Al, (b) TiH_2-30wt% Al, (c) TiH_2-40wt% Al, (d) TiH_2-50wt% Al, (e) TiH_2-60wt % Al.

The dimensions of the cylinders were measured before and after sintering to determine the volume contraction or volume expansion. The cylinders before and after the sintering processes were characterized by X-ray diffraction (XRD, DLMAX-2200, Rigaku, Japan) to identify the crystalline phases. The pore structure before sintering was characterized by optical microscope (OM), while the pore structure after sintering was observed by OM and scanning electron microscopy (SEM, Zeiss SIGMA Field Emission SEM, Germany) with electron backscatter diffraction (EBSD) and energy-dispersive X-ray spectroscopy (EDX, Oxford EBSD and EDX System). After coating the specimen surfaces with paraffin to prevent the penetration of water into the specimen, the overall porosity of the porous cylinders was measured using the Archimedes method. The open porosity was evaluated by measuring the weight and volume of the paraffin that penetrated into the porous cylinders when they were boiled in the paraffin. The sintered TiAl alloys cylinders were cut into discs with the thickness of about 3 mm, and then the bubble-point test method was used to measure the maximum pore size (Porolux 1000 porometer, IB-FT GmbH, Germany). According to the standard DIN EN ISO 4022:2006 [20], the gas permeability for nitrogen was also measured using this porometer at room temperature (23 °C). Hereby, the feed pressure was increased up to 2 bar while the permeable side was kept under atmospheric pressure.

In order to investigate the decomposition of TiH_2 and the reactions between the TiH_2–Al powder mixtures during sintering, differential thermal analysis (DTA, NETZSCH STA 409C, Germany) was used to measure the thermal responses of the TiH_2–Al powder mixtures with different Al contents. The samples were heated at a rate of 5 °C/min from 25 °C to 900 °C under an Ar flow.

3. Results and discussion

3.1. Volume contraction and volume expansion

The dimension change during the sintering procedure for the porous TiAl alloys system is one of the most remarkable phenomena observed in studies of TiAl alloys [4,6,7,18]. Fig. 3 shows the volume and dimension expansion ratios (the volume/dimension of the cylinders after sintering divided by the volume/dimension of the un-sintered cylinders) as a function of the Al content. As seen from Fig. 3, the volume expansion of the cylinder with 20 wt% Al content was about −8% (volume contraction). The reason for this is that the lots of micron-gaps formed by H_2 which was released from the dehydrogenation of TiH_2 below the first holding platform (630 °C), after that shrinkage occurred at the second holding platform (1200 °C). In order to estimate the volume loss

Table 1
Crystalline phases in the sintered samples with different compositions measured by XRD.

Compositions	Phases
TiH_2-20wt% Al	α_2-Ti_3Al, Ti
TiH_2-30wt% Al	α_2-Ti_3Al, γ-TiAl
TiH_2-40wt% Al	α_2-Ti_3Al, γ-TiAl
TiH_2-50wt% Al	$TiAl_3$, Ti_2Al_5
TiH_2-60wt% Al	$TiAl_3$, Al

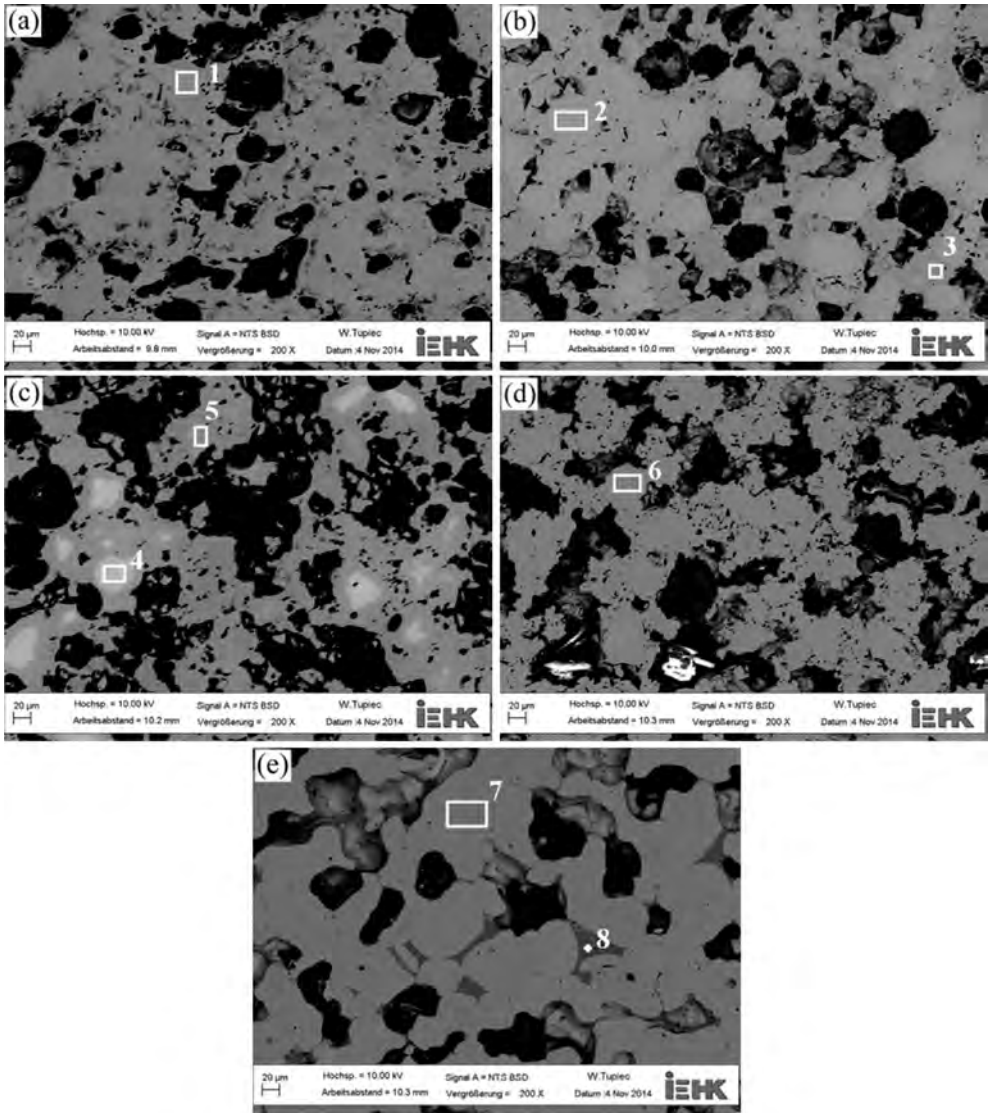

Fig. 7. Backscatter diffraction images of porous TiAl alloy cylinders after sintering: (a) TiH_2-20wt% Al, (b) TiH_2-30wt% Al, (c) TiH_2-40wt% Al, (d) TiH_2-50wt% Al, (e) TiH_2-60wt% Al.

(contraction) caused by the dehydrogenation of TiH_2, 100 wt% TiH_2 powders were sintered using the same procedure. The volume contraction was 27.5%, as shown in Fig. 3. As shown in Fig. 4, the DTA plots show two exothermal peaks, which indicates that the dehydrogenation of TiH_2 occurs in a two-step process as $TiH_2 \rightarrow TiH_x \rightarrow \alpha$-Ti, where $0.7 < x < 1.1$ [19]. Meanwhile, the great heat released by the dehydrogenation of TiH_2 can lead to local Al melting, which leads to an instantaneous reaction between solid Ti and liquid Al. Al melt then flows away along Ti particles or grain boundaries, leaving pores behind [21]. On the other hand, through preferential diffusion of Al atoms into the Ti particles, as a result of the Kirkendall effect [6,21,22], the intermetallic compound $TiAl_3$ on the surfaces of the titanium particles forms. Consequently, particle volume increases. For this reason, the volume contraction of the sample with 20 wt% Al decreased to −8%. According to A.P. Savitskii's work on the reaction sintering of Ti–Al powder mixtures [6,23], the reaction between solid Ti and liquid Al is a strongly exothermic process. However, because the amount of Al melt is not very large and the reaction rate is so high that it cannot be resolved by calorimetry, the exothermal peak cannot be observed clearly [24]. Taking into consideration the temperature profile (Fig. 2), below the temperature of the first holding platform, the temperature of the compact may be higher than that in the furnace. Afterwards, the temperature of the compact could be cooled to 630 °C during the first holding platform. As shown in Fig. 4, with increasing temperature, in the case of TiH_2-50wt% Al and TiH_2-60wt% Al only, tiny exothermal peaks could be seen, which practically overlapped with the melting peak of Al, which indicated that the liquid Al covering the Ti particles had become saturated. This meant that the temperature of the compact was probably not

Table 2
The composition of the selected area in Fig. 7(a)–(e) measured by EDX.

Selected area	Ti (wt%)	Al (wt%)	O (wt%)	Phase
1 (20 wt% Al)	80	20	–	α_2-Ti_3Al
2 (30 wt% Al)	81	19	–	α_2-Ti_3Al
3 (30 wt% Al)	66	34	–	γ-TiAl
4 (40 wt% Al)	83	17	–	α_2-Ti_3Al
5 (40 wt% Al)	61	39	–	γ-TiAl
6 (50 wt% Al)	45	55	–	$TiAl_3$, Ti_2Al_5
7 (60 wt% Al)	37	63	–	$TiAl_3$
8 (60 wt% Al)	2	95	3	Al

higher than the temperature in the furnace during the second heating process.

For Al contents from 30 wt% to 50 wt%, the volume expansions increased almost linearly as the Al content increased. The maximum volume expansion ratio reached about 65% when the Al content was 50 wt%. With increasing higher Al content, the Al melt formed comparatively rigid skeleton forms in the compact and flowed away along the Ti particles or grain boundaries, which enabled it to increase rapidly in size as a result of a diffusional growth of the titanium particles [6,23,25]. Therefore, the volume expansion caused by the flowing away of Al melt increased as the amount of Al melt was increased. In the case of TiH_2-60wt% Al, the volume expansion reduced to about 22%. For this sample, Al was oversupplied to form the $TiAl_3$ phase, which was confirmed by the XRD patterns and EDX results mentioned in next section. After exceeding the melting point of Al, the Al melts were excessive and resulted in the shrinkage of the sintered grains due to the surface tension of the liquid phase [26]. Meanwhile, this blocked the pores formed between the sintered grains. Consequently, these synergetic effects led to the reduction of the volume expansion for the TiH_2-60wt% Al sample. The axial and radial expansion behaviors were also shown to be similar to the behavior of the volume expansion. The maximum axial and radial expansion ratios at the Al content of 50 wt% were ~16% and ~19%, respectively.

3.2. Phase identification

Fig. 5 presents the XRD patterns of green cylinders after CIP with different Al contents. As can be expected, only the Al and TiH_2 phases existed in all the samples before sintering. Fig. 6 shows the XRD patterns after sintering, and six different phases were found in five samples with different Al contents, which is also listed in Table 1. Furthermore, the phases in the sintered samples were confirmed by EBSD and EDX, as shown in Fig. 7 and listed in Table 2. For the sintered cylinder of TiH_2-20wt% Al, only the α_2-Ti_3Al phase was detected, as shown in Fig. 7(a). For the samples of TiH_2-30wt%

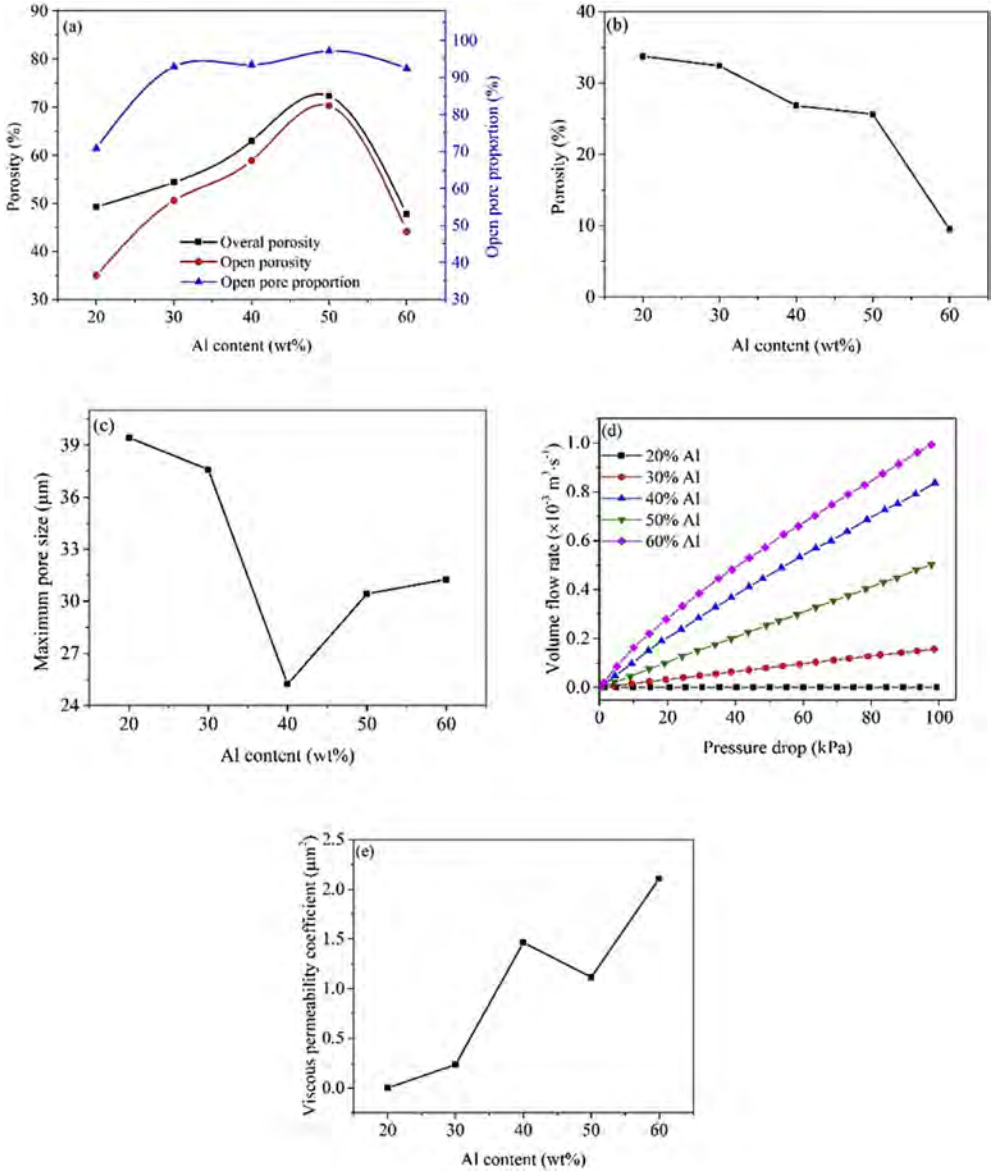

Fig. 8. The relationships between pore properties and the Al content of the porous TiAl alloys: (a) overall porosity, open porosity, and open pore proportion after sintering, (b) porosity before sintering, (c) maximum pore size, (d) nitrogen permeability, (e) viscous permeability coefficient.

Al and TiH_2-40wt% Al, the γ-TiAl and α_2-Ti_3Al phases were observed, as shown in Fig. 7(b)–(c). For the sintered cylinder of TiH_2-50wt% Al, the $TiAl_3$ and Ti_2Al_5 phases could be found by BSD and EDX, as shown in Fig. 7(d). For the sample of TiH_2-60wt% Al, the $TiAl_3$ and Al phases were present, as shown in Fig. 7(e). It can be seen that no free Al was observed except in the sample of TiH_2-60wt% Al. Moreover, it should also be pointed out that the existence of six different phases didn't well match the phases found through the Ti–Al binary phase diagram [27] for the same compositions, especially for the Ti_2Al_5 phase. The reason may be that the sintering and cooling processes are different from the equilibrium solidification process. Besides, the H_2 released from TiH_2 could influence the formation of Ti–Al intermetallic compounds, which will be investigated in the future.

3.3. Pore structure

Apart from the effect on the volume expansion of sintered porous TiAl alloys, the TiH_2 and Al contents also affected the pore structure of the porous TiAl alloys, which is an important factor for practical use, especially when aiming to filter parts of the alloys. In general, two key parameters are used to comprehensively describe the pore structural properties, i.e., the open porosity and maximum pore size.

Fig. 8(a) shows the relationships between the overall and open porosities of the porous TiAl alloys and the Al/TiH_2 content. It should be noted that the result of open porosity could be biased against the real one. The reason for this is that the Archimedes method using paraffin tends to exclude the fine pores. It was found that a certain amount of closed pores exist because the interparticle pores in the green compacts could not be avoided. Fig. 9 shows the microstructure of the green compact cylinders before sintering. In Fig. 9, the white areas are attributed to Al particles, the gray areas to TiH_2 particles, and the black gaps among the particles are the interparticle pores. Due to the more irregular shape of TiH_2 powders compared to Al powders, more interparticle pores were created in the green compacts, which can be confirmed by the change in the porosity with an increasing hydride ratio of the green compacts before sintering. As shown in Fig. 8(b), the porosity of the green compacts before sintering decreased as the aluminum content increased.

Similar to the relationship between the volume expansion and

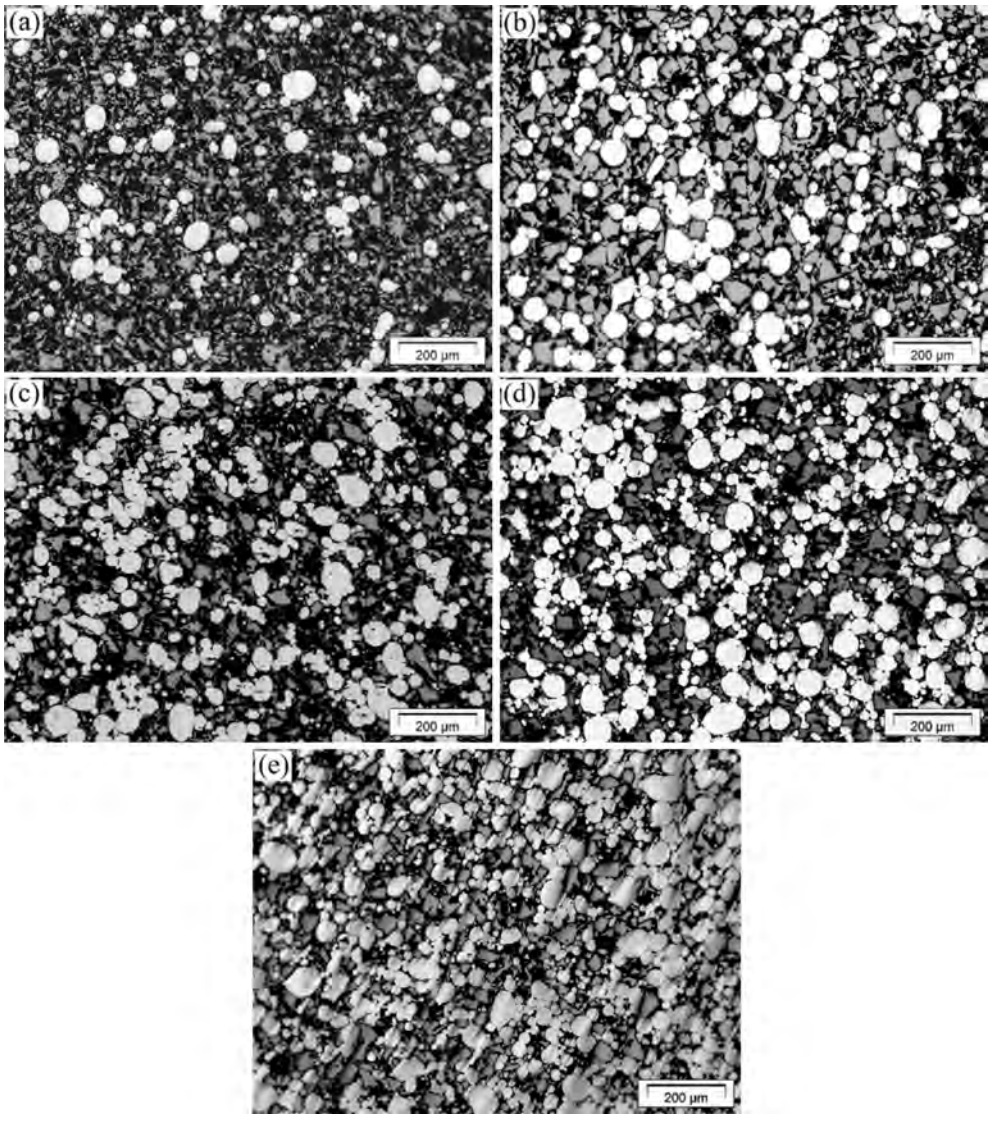

Fig. 9. Microstructure of the green compact cylinders before sintering: (a) TiH_2-20wt% Al, (b) TiH_2-30wt% Al, (c) TiH_2-40wt% Al, (d) TiH_2-50wt% Al, (e) TiH_2-60wt% Al.

the Al content for the sintered samples, the open porosity increased as the Al content rose up to 50 wt%. The maximum open porosity of the porous TiAl alloys was about 70% at the composition of TiH_2-50wt% Al. This indicates that the pores were initiated by the consumption of the Al during the reactive sintering. After that, the open porosity began to reduce gradually. The reason for this is that the excessive Al melt coats over the $TiAl_3$ grains and blocks the pores that are formed between the sintered grains. As a result, the open porosity and overall porosity decreases.

The mechanisms of pore formation can be demonstrated as follows: (1) The pores are initiated from the consumption of Al during the reactive sintering in accordance with the pore formation mechanism caused by the Kirkendall effect [6,21,22]. Since the Al atoms move into Ti particles, whereas the Ti atoms remain almost immobile [5], the movement (consumption) of Al atoms must be balanced by the vacancies. As a result, a large number of vacancies form at the original positions of the Al atoms and the excessive vacancies condense into pores to reduce the system's Gibbs free energy [4], i.e., the reaction between Al and Ti results in the formation of smaller pores directly. (2) With increasing temperature, the dehydrogenation of TiH_2 occurs first and lots of micron-gaps form because of the release of H_2. Meanwhile, because of the great heat given out by the dehydrogenation of TiH_2, the local Al melts and leads to an instantaneous reaction between the solid Ti and the liquid Al. The Al melt then flows away along Ti particles or grain boundaries to spread over the Ti particles, leaving larger pores behind. As a result, the contact surface between Ti and Al is enlarged and the reaction between the solid Ti and the liquid Al is accelerated [21,24]. Therefore, more smaller pores caused by the Kirkendall effect form. (3) At temperatures above the melting point of Al, the liquid Al becomes saturated before all the initial pores are eliminated, and the transition of the solid phase into the melt ceases and densification stops. As a result, the residual pores are contained [28]. For the sample with 60 wt% Al, residual porosity existed due to the existence of the residual Al phase, which was confirmed by XRD and EDX.

The maximum pore size of the porous TiAl alloys as a function of Al content is shown in Fig. 8(c). When the Al content was less than 40 wt%, the maximum pore size decreased as the Al content increased; when the Al content was more than 40 wt% and less than 60 wt%, the result was the opposite. On the one hand, the decomposition reaction of TiH_2 formed some pores and more TiH_2

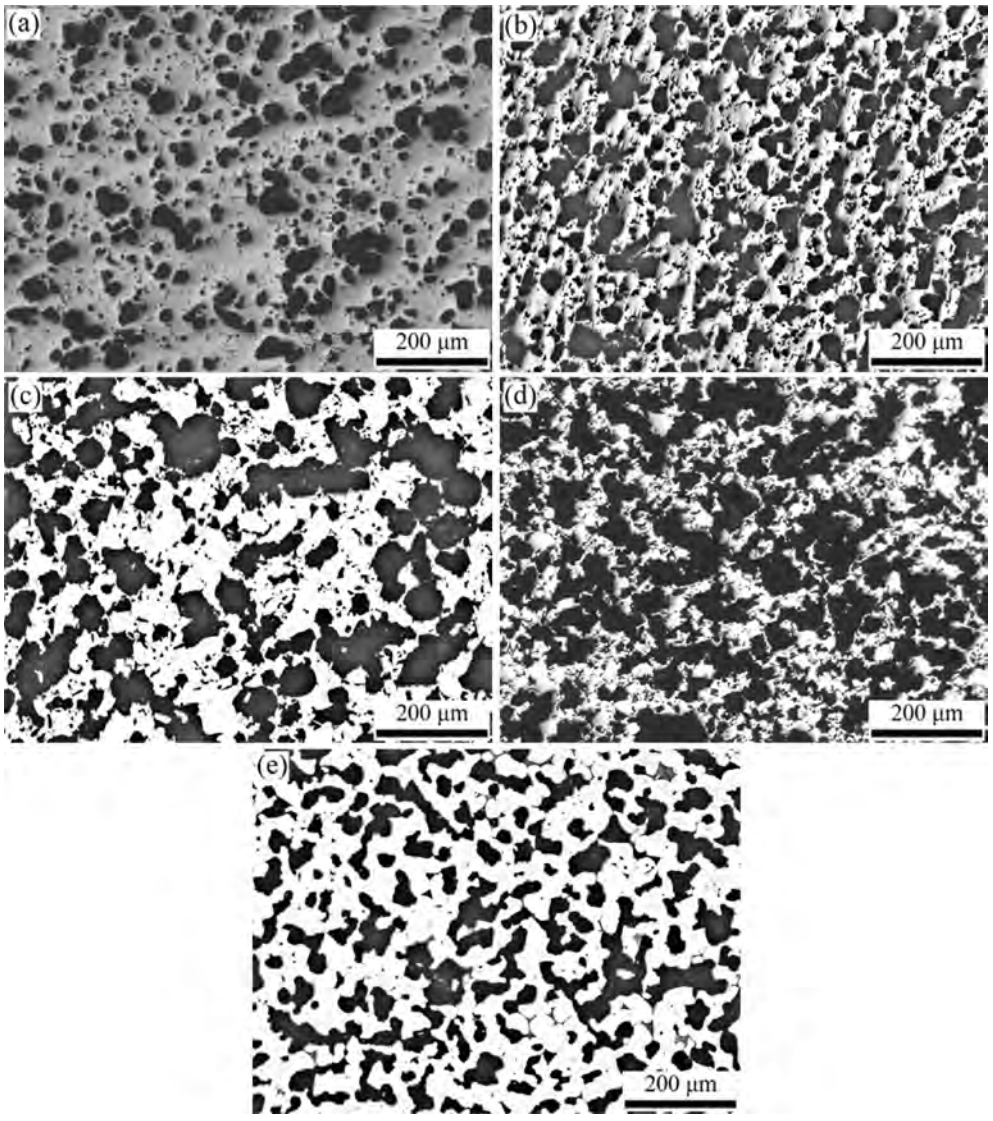

Fig. 10. Pore microstructure of the porous TiAl alloys after sintering: (a) TiH_2-20wt% Al, (b) TiH_2-30wt% Al, (c) TiH_2-40wt% Al, (d) TiH_2-50wt% Al, (e) TiH_2-60wt% Al.

powder, leading to a larger pore size. Besides this, the proportion of open pores increased as the Al content increased (see Fig. 8(a)). On the other hand, if the number of Al powders had been significantly greater than the number of Ti powders, an agglomeration behavior of Al powders would have occurred, and this would have enlarged the practical size of the Al particles. Since pores were mainly generated from the exhaustion of Al, as mentioned in the mechanisms of pore formation (2), the larger Al particle size led to the formation of larger pores. When the Al content was less than 40 wt %, the effect of TiH_2 decomposition on the maximum pore size was dominant. However, the effect of the exhaustion of Al was dominant when the Al content was over 40 wt%. It should be mentioned that for the sample with 60 wt% Al, the maximum pore size continued to increase even if some residual Al existed and led to a reduction of the porosity. In addition, Fig. 10 shows the OM images of five porous TiAl alloys with different Al contents after sintering. In Fig. 10 the bright areas are attributed to mixtures and the dark areas are attributed to pores. As can be clearly seen, the general pore size increased as the Al content increased when the Al content was less than 50 wt%. After that, the pore size began to reduce at the Al content of 60 wt%.

3.4. Gas permeability/filter performance

As a porous medium, viscous permeability plays an important role in filter performance. According to the standard DIN EN ISO 4022:2006 [20], gases are more suitable than liquids for the determination of the viscous permeability coefficient ψ_v. For a laminar flow regime, the incompressible fluid flow in a porous medium is governed by Darcy's law, in which the permeability can be evaluated using:

$$Q = \frac{\psi_v A}{\eta e}\Delta P, \quad (1)$$

where Q is the volume flow rate, A is the cross-sectional area (2.83×10^{-4} m^2), e is the thickness of the sample (3 mm), η is the dynamic viscosity of the fluid (N_2, $\eta = 1.766 \times 10^{-5}$ Pa s [29] at room temperature), and ΔP is the pressure drop from the entrance to the exit of the sample. As shown in Fig. 8(d), the pressure drop versus the volume flow rate curves were experimentally determined. The plots of Q as a function of ΔP for different Al content samples are linear and can be demonstrated with a straight line. This linearity indicates that the flow was in the laminar flow regime and that Darcy's law was applicable to our samples. Using Eq. (1), the viscous permeability coefficients were calculated from the slope of the line plotted for ΔP versus Q. The result is shown in Fig. 8(e). It can be seen that the gas permeability increased as the Al content increased. Except for the samples with 20 wt% and 30 wt% Al, the viscous permeability coefficients of other porous TiAl alloys samples were sufficient for the solid-to-gas separation applications (from 1.46 μm^2 for the TiH_2-40wt% Al to 2.11 μm^2 for the TiH_2-60wt % Al).

4. Conclusions

Porous TiAl alloys parts for filter applications with nominal compositions ranging from TiH_2-20wt% Al to TiH_2-60wt% Al were successfully fabricated by the reactive synthesis of TiH_2 and Al elemental powders using the PM method. By increasing the Al contents (and, vice versa, decreasing the TiH_2 contents), four intermetallic phases were observed in the sintered porous TiAl alloys: α_2-Ti_3Al, γ-TiAl, $TiAl_3$, and Ti_2Al_5. The effects of the Al content (TiH_2 content) on the pore properties, including open porosity, maximum pore size, and gas permeability, were comprehensively determined. Moreover, the formation mechanisms of pores were demonstrated according to different Al contents. An optimal composition of TiH_2-50wt% Al was defined, as its maximum open porosity was about 70% and its viscous permeability coefficient for nitrogen was 1.11 μm^2. One of the advantages of these porous TiAl alloys over conventional porous materials is that they can be fabricated using a cost-effective and simple PM method.

Acknowledgments

Q.P. gratefully acknowledges the support from the China Scholarship Council (No. 2011689004). The Authors acknowledge the help of T. Schreiner with operating the CIP machine and the help of O. David with operating the bubble point test. The authors thank A.M. Khamoushkoo for designing the gas tight container for the sintering process.

References

[1] H. Nakajima, Fabrication, properties and application of porous metals with directional pores, Prog. Mater. Sci. 52 (2007) 1091–1173.
[2] L.-P. Lefebvre, J. Banhart, D. Dunand, Porous metals and metallic foams: current status and recent developments, Adv. Eng. Mater. 10 (2008) 775–787.
[3] P. Liu, K. Liang, Review functional materials of porous metals made by P/M, electroplating and some other techniques, J. Mater. Sci. 36 (2001) 5059–5072.
[4] Y.H. He, Y. Jiang, N.P. Xu, J. Zou, B.Y. Huang, C.T. Liu, et al., Fabrication of Ti-Al micro/nanometer-sized porous alloys through the Kirkendall effect, Adv. Mater. 19 (2007) 2102–2106.
[5] F. Van Loo, G. Rieck, Diffusion in the titanium-aluminium system – I. Interdiffusion between solid Al and Ti or Ti-Al alloys, Acta Metall. 21 (1973) 61–71.
[6] A. Savitskii, N. Burtsev, Dilatometric investigations of the growth of Ti-Al compacts during liquid-phase sintering, Powder Metall. Metal Ceram. 22 (1983) 176–181.
[7] G.-X. Wang, M. Dahms, Influence of heat treatment on microstructure of Ti-35wt.% Al prepared by elemental powder metallurgy, Scripta Metall. Mater. 26 (1992) 717–722.
[8] M. Yamaguchi, H. Inui, K. Ito, High-temperature structural intermetallics, Acta Mater. 48 (2000) 307–322.
[9] H. Clemens, S. Mayer, Design, processing, microstructure, properties, and applications of advanced intermetallic TiAl alloys, Adv. Eng. Mater. 15 (2013) 191–215.
[10] H. Clemens, Intermetallic γ-TiAl based alloy sheet materials: processing and mechanical properties, Z. für Met. 86 (1995) 814–822.
[11] H. Clemens, H. Kestler, Processing and applications of intermetallic γ-TiAl-based alloys, Adv. Eng. Mater. 2 (2000) 551–570.
[12] Z.S. Rak, J. Walter, Porous titanium foil by tape casting technique, J. Mater. Process. Technol. 175 (2006) 358–363.
[13] C.R.F. Azevedo, D. Rodrigues, F.B. Neto, Ti-Al-V powder metallurgy (PM) via the hydrogenation-dehydrogenation (HDH) process, J. Alloys Compd. 353 (2003) 217–227.
[14] Z. Tang, F. Wang, W. Wu, Hot-corrosion behavior of TiAl-base intermetallics in molten salts, Oxid. Metals 51 (1999) 235–250.
[15] J. Lapin, Creep behaviour of a cast TiAl-based alloy for industrial applications, Intermetallics 14 (2006) 115–122.
[16] X. Wu, Review of alloy and process development of TiAl alloys, Intermetallics 14 (2006) 1114–1122.
[17] R. Schnitzer, H.F. Chladil, C. Scheu, H. Clemens, S. Bystrzanowski, A. Bartels, et al., Herstellung lamellarer Gefügetypen in intermetallischen TiAl-Legierungen und deren Charakterisierung, Pract. Metallogr. 44 (2007) 430–442.
[18] Y. Jiang, Y.H. He, N.P. Xu, J. Zou, B.Y. Huang, C.T. Liu, Effects of the Al content on pore structures of porous Ti-Al alloys, Intermetallics 16 (2008) 327–332.
[19] V. Bhosle, E. Baburaj, M. Miranova, K. Salama, Dehydrogenation of TiH_2, Mater. Sci. Eng. A 356 (2003) 190–199.
[20] DIN EN ISO 4022:2006, Permeable Sintered Metal Materials – Determination of Fluid Permeability, Beuth Verlag GmbH, 2006.
[21] G.-X. Wang, M. Dahms, An effective method for reducing porosity in the titanium aluminide alloy $Ti_{52}Al_{48}$ prepared by elemental powder metallurgy, Scripta Metall. Mater. 26 (1992) 1469–1474.
[22] T. Lee, E. Mosunov, S. Hwang, Consolidation of a gamma TiAl-Mn-Mo alloy by elemental powder metallurgy, Mater. Sci. Eng. A 239 (1997) 540–545.
[23] A. Savitskii, N. Burtsev, Effect of powder particle size on the growth of titanium compacts during liquid-phase sintering with aluminum, Soviet Powder Metall. Metal Ceram. 20 (1981) 618–621.
[24] G.-X. Wang, M. Dahms, G. Leitner, S. Schultrich, Titanium aluminides from cold-extruded elemental powders with Al-contents of 25-75 at% Al, J. Mater. Sci. 29 (1994) 1847–1853.
[25] A. Savitskii, N. Burtsev, Compact growth in liquid-phase sintering, Powder Metall. Metal Ceram. 18 (1979) 96–102.

[26] G. Schaffer, T. Sercombe, R. Lumley, Liquid phase sintering of aluminium alloys, Mater. Chem. Phys. 67 (2001) 85–91.
[27] Alloy Phase Diagrams. Handbook, Aerospace Structural Metals, ASM Int. Mater. Park., Ohio, 1992.
[28] O. Lapshin, A. Savitskii, V. Ovcharenko, Mathematical model of compact changes in volume during liquid-phase sintering. II, J. Mater. Synth. Process. 9 (2001) 83–92.
[29] W.A. Cole, W.A. Wakeham, The viscosity of nitrogen, oxygen, and their binary mixtures in the limit of zero density, J. Phys. Chem. Ref. Data 14 (1985) 209–226.